Sulfur 1s core-level photoionization of SF_6

T. A. Ferrett, D. W. Lindle, P. A. Heimann, H. G. Kerkhoff,* U. E. Becker,* and D. A. Shirley
Materials and Molecular Research Division, Lawrence Berkeley Laboratory and Department of Chemistry, University of California, Berkeley, California 94720
(Received 12 February 1986)

Photoelectron spectra have been taken between 2460 and 2600 eV photon energy across the discrete and continuum resonances in the vicinity of the sulfur K edge in gaseous SF_6. Results at the below-threshold S $1s \rightarrow 6t_{1u}$ resonance indicate that "highly excited" S $2p$ and S $2s$ satellites (with two core holes) are the primary autoionization final states of SF_6^+. An observed asymmetric profile in the S(LVV) Auger angular distribution suggests interference effects in the alignment of these resonantly produced SF_6^+ ions. Decay of the low-energy S $1s$ continuum resonances near 2507 eV photon energy into S $2p$, S $2s$, and/or valence photoemission channels indicates autoionizing character. These features are assigned as doubly excited states, leading to S $1s$ satellite thresholds observed here for the first time. At higher photon energies, between 2520 and 2570 eV, large oscillations in the S $1s$ cross section are reproduced well by multiple-scattering $X\alpha$ calculations, but are not explained adequately by single-scattering plane-wave extended x-ray absorption fine structure effects. We speculate that improvements in the description of both the electron scattering process and the molecular potential are necessary to model the diffractive and nondiffractive (barrier interaction) effects in this energy region.

I. INTRODUCTION

When the first gas-phase photoabsorption measurement near the sulfur K edge in SF_6 (reproduced in Fig. 1) was published in 1966, the appearance of the spectrum was described as being "unusually rugged" from the S $1s$ threshold (2490 eV) up to about 2570 eV photon energy.[1] Several years later, a lineup of the S $1s$, S $2p$, and F $1s$ core-level photoabsorption spectra of SF_6 referenced to their respective ionization thresholds revealed an interesting correlation of the resonant features in kinetic energy to within a few eV.[2,3] This correlation led to the assignment of continuum features in these spectra as e_g and t_{2g} shape resonances,[3,4] and in particular suggested that some of the "rugged" continuum features in the S $1s$ spectrum were related to potential-barrier effects.

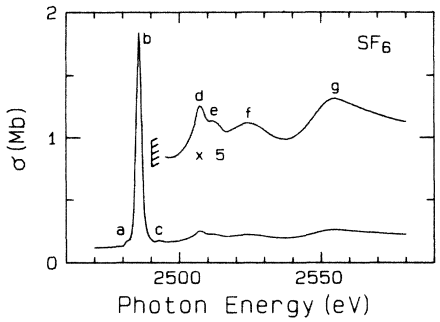

FIG. 1. Photoabsorption spectrum of SF_6 near the S $1s$ threshold (2490 eV) from Ref. 1. The features discussed in the text are the S $1s \rightarrow 6t_{1u}$ resonance (b), the resonances near 2507 eV (d and e), and the higher-energy features (f and g). Features a and c are not discussed in this work, but have been interpreted as the symmetry-forbidden transitions S $1s(1a_{1g}) \rightarrow 6a_{1g}$ (a) and εt_{2g} (c) (Ref. 3).

Theoretically, there have been major advances in the basic understanding of potential-barrier effects in atoms[5-8] and, initially with the application of the multiple-scattering method (MSM-$X\alpha$), in molecules.[9-15] In a simple one-electron model, a shape resonance is a pure final-state effect. It should thus occur at approximately the same kinetic energy for different core levels of a given molecule. The continuum electron can be pictured as being trapped temporarily by a centrifugal barrier, producing a resonance at a kinetic energy roughly comparable to the barrier height. The large observed photoabsorption intensities of discrete states also fit into this scheme; the unusual potential can enhance the discrete molecular-orbital transitions at the expense of Rydberg excitations and nonresonant continuum intensity. Because the core-level spectra of SF_6 exhibit strong resonances that have been associated with an unusually high potential barrier,[3,4] SF_6 has become a prototypical example of potential-barrier effects and shape resonances.[16]

The present assignments for the S $1s$ absorption spectrum of SF_6 shown in Fig. 1 are as follows. We use the letter assignments in Fig. 1 throughout the paper to refer to features a–g. The interpretation of the only intense below-threshold resonance (b) as a discrete excitation of a S $1s$ electron to the unoccupied $6t_{1u}$ level is straightforward.[3] The SF_6 energy-level diagram in Fig. 2 illustrates this transition. For the S $1s$ continuum, the shape-resonance model was used to assign two features at $\sim$2493 (c) and 2506 eV (d) photon energy.[3] However, this interpretation is not so straightforward because these transitions [S $1s(1a_{1g}) \rightarrow t_{2g}, e_g$] are symmetry forbidden in the simple shape-resonance picture.[3] Furthermore, we note that assignment of resonance features based solely on

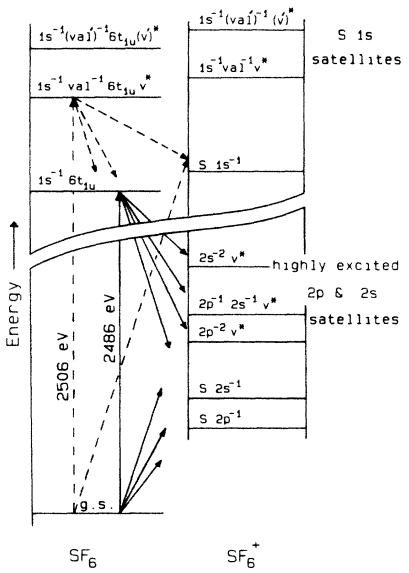

FIG. 2. Sulfur 1s resonance energy-level diagram for SF_6. The $1s^{-1}6t_{1u}$ neutral excited state and its available photoemission decay channels to SF_6^+ are shown with solid lines. Note the presence of highly excited S 2p and S 2s satellites produced by decay of the $1s^{-1}6t_{1u}$ state. Two postulated doubly excited states (see text for details) of the neutral are shown also, with some of the corresponding decay channels illustrated by dotted lines. Some excitation and decay pathways have been omitted for clarity. The designations val and v^* represent outer-valence orbitals, and either $6a_{1g}$ or $6t_{1u}$ orbitals, respectively.

photoabsorption data can be uncertain; effects due to satellite continua and doubly excited resonances may not be distinguishable from those caused by continuum shape resonances.[17,18] Finally, the nature of the higher-energy features (*f* and *g*) remains unexplained.

To examine in more detail the core-level excitation of the "classic" potential-barrier molecule, we undertook a gas-phase photoemission study of the features near the sulfur *K* edge of SF_6 using synchrotron radiation and time-of-flight electron analysis. By investigating the behavior of the individual photoemission channels, we hoped to ascertain the nature of the rugged continuum structure and the autoionization decay characteristics of the S $1s \rightarrow 6t_{1u}$ discrete resonance. No other photoemission measurements have been reported on the S and F core levels in SF_6, but related gas-phase[19,20] and condensed-phase[21] photoemission experiments on the outer-valence orbitals in the photon-energy range 10–54 eV have been reported. These low-photon-energy results show that the assigned t_{2g} shape resonance exhibits unusual behavior by coupling to neighboring symmetry-forbidden valence channels.[19–21] In addition, the lack of evidence for the e_g shape resonance in the valence subshells remains puzzling.

Related core-level photoemission results in other molecules include recent studies of autoionization below the carbon and nitrogen *K* edges of CO and N_2. These studies have revealed interesting decay channels leading to singly charged ions, identified by peaks termed "spectator" satellites.[22–25] The dominance of these channels is rationalized as follows. A core-level electron is promoted to an unoccupied molecular orbital and remains as a spectator while the remaining electrons decay, with one electron filling the core hole and a second electron being ionized.[24,26] The singly charged ion configurations thus produced contain an excited electron and *two* valence holes; these final states are therefore valence satellites. This autoionization decay of the excited neutral in some cases may parallel the Auger decay of the corresponding ion with the excited electron removed.

We observe similar spectator satellite decay channels at the S $1s(1a_{1g}) \rightarrow 6t_{1u}$ excitation (*b*) below the S 1s threshold of SF_6. The satellites produced contain S 2p and/or S 2s vacancies. In addition, the subsequent relaxation of the resonantly produced SF_6^+ ions via Auger decay of the *L* holes permits the measurement of the Auger-electron cross sections and, of more interest, the angular distribution asymmetry parameter β. We report the first measurement of the angular distribution of Auger electrons from an ion produced by an autoionization process. Autoionization can produce aligned +1 ions, and the subsequent Auger decay can retain some memory of this alignment, which may affect the Auger β.[27] No previous angular-distribution measurements have been performed at photon energies high enough such that the single ions produced by autoionization are energetically able to Auger decay.

Turning to the S 1s continuum in SF_6, we have examined the resonant features in the vicinity of 2507 eV (*d* and *e*) and at higher energies (*f* and *g*). The results near 2507 eV demonstrate that these resonant states decay into channels other than the S 1s continuum (e.g., S 2p, S 2s, valence). This decay pattern, combined with the observation of S 1s correlation-satellite thresholds slightly higher in energy, suggest assignment of these features as arising from doubly excited states.

In order to explain the higher-energy effects and the large oscillations in the cross section between 30 and 70 eV kinetic energy (*f* and *g*), the application of recent advances in extended x-ray absorption fine structure (EXAFS) theory, including spherical-wave[28–31] and multiple-scattering corrections,[28,31–35] would probably be required. In addition, we propose that the details of the molecular potential also are important for intermediate-energy electrons which can interact significantly both with the diffuse electron cloud (large *r*) and with the localized atomic centers (small *r*). Our interpretation of the S 1s continuum generally indicates that the kinetic energy region 30–100 eV is especially complicated and probably displays neither simple shape-resonance nor EXAFS behavior.

The experimental details of this work are presented in Sec. II. In Sec. III, we lay the groundwork for interpretation of the results by describing our photoemission spectra. We discuss the results for the S $1s \rightarrow 6t_{1u}$ below-threshold resonance in Sec. IV, and for the S 1s continuum in Sec. V. Our conclusions appear in Sec. VI.

II. EXPERIMENTAL

The experiment was performed at the Stanford Synchrotron Radiation Laboratory (SSRL) using photons

from JUMBO, a double-crystal monochromator operating with Ge(111) crystals on beam line III-3. Synchrotron radiation photoionized an effusive beam of SF_6 molecules, and Auger electrons and photoelectrons were detected at 0° and 54.7° relative to the photon polarization direction using the double-angle time-of-flight (DATOF) method.[36–38] This method takes advantage of the time structure of the Stanford positron-electron accelerator storage ring (SPEAR) and allows determination of relative partial cross sections, branching ratios, and angular distributions for Auger electrons and photoelectrons.

The angular distribution of photoelectrons from a randomly oriented sample using a linearly polarized photon source can be described in the dipole approximation by Yang's theorem as[39]

$$\frac{d\sigma(h\nu,\theta)}{d\Omega}=\frac{\sigma(h\nu)}{4\pi}[1+\beta(h\nu)P_2(\cos\theta)], \quad (1)$$

where θ is the angle between the photon polarization and the electron emission direction, $P_2(\cos\theta)$ is the second Legendre polynomial, and $\sigma(h\nu)$ and $\beta(h\nu)$ are the partial cross section and angular distribution asymmetry parameter, respectively. At the magic angle of $\theta=54.7°$, peak intensities are proportional to the partial cross section $\sigma(h\nu)$. In order to measure $\beta(h\nu)$, it suffices to detect electrons at only one other angle, 0° in our case. The degree of linear polarization assumed in Eq. (1) is 100%. The polarization of the photons from JUMBO is unknown, but probably somewhat greater than 90%. This uncertainty leads to an absolute error in the β values reported here of less than ±0.05 because of our calibration procedure.[37] Finally, though the dipole approximation is assumed valid for this experiment, deviations may occur with very-high-energy photons in the keV range. However, such effects should be small for these particular measurements, where the dipole processes are strong.

Peak intensities obtained at 54.7° must be corrected for fluctuations in sample pressure and photon intensity in order to determine relative partial cross sections. The photon intensity was monitored by measuring the total electron yield of graphite with a channeltron placed at the back of the sample chamber. A 1500-Å-thick Al window separated the monochromator vacuum (10^{-10} torr) from the sample-chamber pressure (10^{-4} torr), which was recorded with a capacitance manometer. We estimate that systematic errors in our relative cross section (not represented by the statistical error bars in our plots) are 10% or less.

Time-of-flight spectra were taken from $h\nu=2460$ to 2600 eV with a monochromator bandpass of about 2.4 eV. Energy calibration of the monochromator was accomplished by scanning over the below-threshold resonance (S $1s\rightarrow 6t_{1u}$) in SF_6 at 2486 eV.[1] The 54.7° analyzer transmission as a function of electron kinetic energy was determined using atomic argon, by comparing Ar $1s$ photoemission intensity to Ar LMM Auger intensity. Variations in this ratio were attributed to changes in the analyzer transmission at the kinetic energy of the Ar $1s$ peak. The asymmetry-parameter measurements were calibrated in the kinetic energy range of about 7–100 eV by measuring the Ar $1s$ peak at varying kinetic energies, and assuming the β(Ar $1s$)=2.0. At intermediate kinetic energies (110–200 eV), the S(LVV) Auger peak was used as a calibrant by assuming arbitrarily a nonresonant β value of zero. For very high kinetic energy electrons (>1800 eV), the F $1s$ photoemission peak in SF_6 was used for calibration with an assumed β of 2.0.

During the experiment there were significant fluctuations in the position of the photon beam which changed the relative analyzer efficiency by as much as 20% and the 54.7° analyzer transmission by a factor of 2. Within a set of spectra unaffected by beam movement, we observed that the intensity and asymmetry parameter for the F(KVV) Auger peak were relatively constant in the photon-energy range 2460–2600 eV. Thus, corrections were made in each spectrum for beam fluctuations using the F Auger peak as a standard. These experimental complications involving the movement of the photon beam also made calibration for the β measurements at low kinetic energies especially difficult, leading to possible systematic errors not represented by the statistical error bars shown in our asymmetry-parameter plots. We estimate that the uncertainty in the S $1s$ β between 2530 and 2550 eV is ±0.15. Likewise, at the lower kinetic energies (below 12 eV), the analyzer efficiency changes dramatically, also increasing the β uncertainty to ±0.15.

A representative S $1s$ time-of-flight spectrum is shown in Fig. 3. Count rates for the S $1s$ peak were 4–30 counts/sec with 1000-sec collection times. There are F $1s$, S $2p$, S $2s$, and valence photoemission contributions to the high-energy peak A, as well as S(KLL, KLV, and KVV) Auger intensity. The relative importance of these components will be discussed in more detail in Sec. III.

III. PEAK CONTRIBUTIONS IN THE S $1s$ PHOTOEMISSION SPECTRA

Interpretation of experimental results in Secs. IV and V requires knowledge of the processes that contribute to the peaks in the S $1s$ photoelectron spectra. These contributions must be considered together because some of them are not resolved in our spectra. The kinetic-energy resolu-

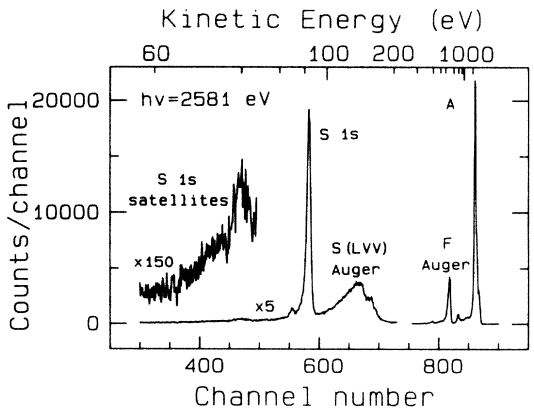

FIG. 3. TOF spectrum of SF_6 taken at $\theta=0°$ and 2581 eV photon energy above the S $1s$ threshold at 2490 eV. The components for peak A are listed in Table I.

tion in the TOF spectra is limited by time dispersion due to the finite dimensions of the photon beam, and to a lesser extent by the time resolution inherent in the time-of-flight technique. For the measurements on the JUMBO monochromator, this corresponds to ~9% of the kinetic energy, or as much as 180 eV at 2000 eV kinetic energy.

The TOF spectrum in Fig. 3, taken 91 eV above the S 1s threshold at 2490 eV, includes the S 1s main-line and satellite peaks, the S(*LVV*) Auger peak, the F(*KVV*) Auger peak, and peak *A*. Figure 4 illustrates a second spectrum taken below the S 1s threshold, showing the very weak S($L_1L_{2,3}V$) Auger peak. Several of the peaks in Fig. 3 arise from only one process at all photon energies used in this study. Specifically, the S 1s main-line and satellite peaks and the peak comprised of the F(*KVV*) Auger transitions remain well-resolved from all other peaks.

There are, on the other hand, several dissimilar components in peak *A* and in the S(*LVV*) and S($L_1L_{2,3}V$) Auger peaks. The processes that contribute to each of these observed peaks in three energy regions are listed in Table I. We define the energy ranges as follows: below the sulfur *K* edge, between the S 1s main-line threshold and the first satellite threshold, and above the first S 1s satellite threshold.

Peak *A* has the most complicated structure because it includes all photoemission main lines and satellites with binding energies less than 700 eV. Below the sulfur *K* edge, the photoemission contributions to peak *A* are from F 1s, S 2s, S 2p, and valence main lines and satellites. Some "highly excited" S 2p and S 2s satellite configurations ($2p^{-2}v^*$, $2s^{-2}v^*$, and $2s^{-1}2p^{-1}v^*$, where the valence state v^* is probably either the $6t_{1u}$ or $6a_{1g}$ molecular orbital) also contribute to peak *A* in the vicinity of the S $1s\rightarrow 6t_{1u}$ resonance at 2486 eV. There is a slight

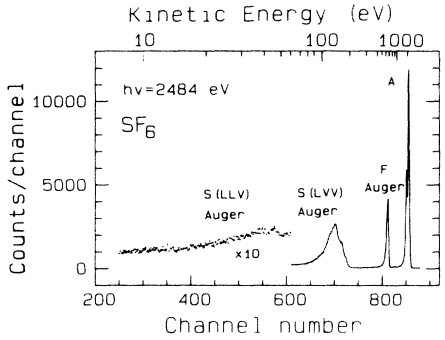

FIG. 4. A TOF spectrum of SF_6 taken at $\theta=54.7°$ and 2484 eV near the S $1s(1a_{1g})\rightarrow 6t_{1u}$ resonance.

double-peak structure to peak *A*, as shown in the spectrum in Fig. 4, because the F 1s peak is at a lower kinetic energy, while the remaining resonant satellite contributions are unresolved at higher energy. Finally, as the photon energy is increased to above the S 1s main-line and S 1s satellite thresholds, the primary Auger decay from S 1s hole states produces high-kinetic-energy S(*KLL*, *KLV*, and *KVV*) Auger electrons which also contribute to the peak-*A* intensity.

Below the sulfur *K* edge, the S($L_{1,2,3}VV$) and S($L_1L_{2,3}V$) peaks result from Auger decay of resonantly and nonresonantly produced SF_6^+ ions ($2s^{-1}$, $2p^{-1}$, $2p^{-2}v^*$, etc.) with S 2p and/or S 2s holes, e.g.,

$$\begin{aligned} &SF_6+h\nu(<2490\text{ eV})\rightarrow SF_6^+(2p^{-1})+e^-, \\ &SF_6^+(2p^{-1})\rightarrow SF_6^{2+}(2p^6\text{val}^{-2})+L_{2,3}VV\text{ Auger }e^-. \end{aligned} \tag{2}$$

The especially complicated Auger decay cascades occurring at the discrete S $1s\rightarrow 6t_{1u}$ resonance will be presented in the next section. In particular, the characteristics of

TABLE I. Peak contributions for the SF_6 S 1s photoelectron spectra.

Photon-energy[a] range	Peak *A*	Peak S(*LVV*) Auger	Peak S($L_1L_{2,3}V$) Auger
<2490 eV	F 1s, S 2p, S 2s, valence (main lines and satellites)	$L_{1,2,3}VV$ Auger decay of S 2p, S 2s holes (main lines and satellites)	Auger decay of S 2s holes (main lines and satellites)
2490–2510 eV	all of above *plus* *KLL*, *KLV*, *KVV* Auger decay of S 1s hole (main line)	all of above *plus* $L_{1,2,3}VV$ secondary Auger decay of S 1s hole (main line)	all of above *plus* secondary Auger decay of S 1s hole (main line)
>2510 eV	all of above *plus* *KLL*, *KLV*, *KVV* Auger decay of S 1s hole (satellites)	all of above *plus* $L_{1,2,3}VV$ secondary Auger decay of S 1s hole (satellites)	all of above *plus* secondary Auger decay of S 1s hole (satellites)

[a]The energy ranges above designate the regions below the S 1s threshold (<2490 eV), between the S 1s main-line and first satellite threshold (2490–2510 eV), and above the first S 1s satellite threshold (>2510 eV).

the Auger decay of aligned SF_6^+ ions produced by autoionization will be discussed.

Moving above the S $1s$ main-line and satellite thresholds, the S(LVV) and S($L_1L_{2,3}V$) Auger peaks include the subsequent decay of S $1s$ hole states, e.g.,

$$\begin{aligned} &SF_6+h\nu(\geq 2490\text{ eV})\rightarrow SF_6^+(1s^{-1})+e^-,\\ &SF_6^+(1s^{-1})\rightarrow SF_6^{2+}(1s^22p^{-2})+KL_{2,3}L_{2,3}\text{ Auger }e^-,\\ &SF_6^{2+}(1s^22p^{-2})\rightarrow SF_6^{3+}(1s^22p^{-1}\text{val}^{-2})\\ &\qquad +L_{2,3}VV\text{ Auger }e^-,\\ &SF_6^{3+}(1s^22p^{-1}\text{val}^{-2})\rightarrow SF_6^{4+}(1s^22p^6\text{val}^{-4})\\ &\qquad +L_{2,3}VV\text{ Auger }e^-. \end{aligned} \tag{3}$$

Note that in the particular example given above, it is also possible to produce a tertiary S($L_{2,3}VV$) Auger electron in the decay of SF_6^{3+} to SF_6^{4+}. Because tertiary and occasionally quaternary Auger decay processes can occur in filling the S $2p$ and S $2s$ core holes, the observed S($L_1L_{2,3}V$) and S(LVV) Auger peaks will include *all* of these emitted Auger electrons. By writing these simple illustrative processes, we do not wish to imply that the complex Auger decay necessarily occurs stepwise. Dissociation has also been ignored in the above scheme, but will be considered later.

The reader is referred to Table I for specific peak contributions in each energy range appropriate to the discussion of results in Secs. IV and V.

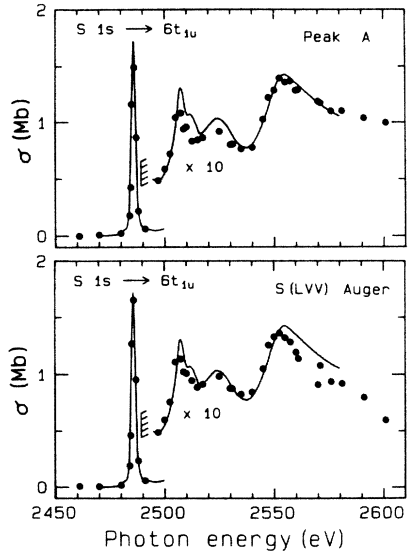

FIG. 5. Peak A (top) and S(LVV) Auger (bottom) relative cross sections and the photoabsorption measurement (Ref. 1, solid curve). The below-threshold nonresonant intensity has been subtracted from the data and the absorption curve. The data have been scaled to the absorption curve at 2497 eV for comparison. The cross-section scale (in Mb) thus refers strictly only to the photoabsorption data, and not to the photoemission and Auger cross sections.

IV. THE BELOW-THRESHOLD S $1s\rightarrow 6t_{1u}$ RESONANCE

For the S $1s\rightarrow 6t_{1u}$ resonance, the possible decay channels to SF_6^+ are described in Sec. IV A. We examine in Sec. IV B the energies and shapes of peak A and the S($L_1L_{2,3}V$) and S(LVV) Auger peaks to deduce qualitatively the important decay channels leading to SF_6^+. We show in Sec. IV C that an analysis of the sulfur Auger cross-section ratio $I(LVV)/I(LLV)$ implies a dominance of a particular single-ion resonant configuration, the $2p^{-2}v^*$ spectator satellite. In Sec. IV D, we present asymmetry-parameter results for peak A and the LVV Auger peak in the S $1s\rightarrow 6t_{1u}$ resonance region. The observed asymmetric profile for the S(LVV) Auger β is discussed with respect to ion alignment[27] and its implications for the Auger-electron angular distribution.

A. Resonant decay channels to SF_6^+

At this resonance, the excited neutral state $1s^{-1}6t_{1u}$ will decay to any continua that are energetically accessible: F $1s$, S $2p$, S $2s$, and valence main-line and satellite final states of SF_6^+.[40] The intensity in peak A below the S $1s$ threshold includes contributions from all of these channels. The below-threshold S $1s(1a_{1g})\rightarrow 6t_{1u}$ resonance appears in the cross section for both peak A and S(LVV) Auger (Fig. 5). The energy-level diagram in Fig. 2 illustrates these decay channels (solid lines).

The many SF_6^+ states to which the excited $1s^{-1}6t_{1u}$ state can autoionize are listed generically in Table II. Our photoemission spectra indicate no resonant enhancement in the F $1s$ channel [as mirrored in the F(KVV) Auger peak], and qualitatively there is very little enhancement of peaks with binding energies below 150 eV. Therefore, we have considered only the SF_6^+ decay channels which have S $2p$ and/or S $2s$ holes. Columns 1—4 of Table II describe these available continuum channels in terms of the configurations, decay types, and approximate binding energies of the states. We use Auger notation in column 3 only to denote the *type* of autoionization decay to each SF_6^+ photoemission channel.[41]

Each available channel can be described as a S $2s$ or S $2p$ main line or satellite. The satellites can be split further into two groups. First, the S $2p$ and S $2s$ satellite configurations with binding energies about 10—40 eV above the respective main-line thresholds have a valence electron promoted to an unoccupied molecular orbital. Decay to the main lines and to these low-excitation photoemission satellites can be viewed as KLV Auger-*type* transitions. Furthermore, the transition can either leave the initially excited $6t_{1u}$ electron as a spectator (KLV) or involve it as a participant (KLV^*) in the decay. In this context, decay to the main-line channel and some satellite channels must involve the excited $6t_{1u}$ electron, while the satellite configurations with a $6t_{1u}$ electron are spectator satellites. The nonresonant intensity for low-excitation-energy satellites may vary from a few percent to as much as 25% relative to the main-line intensity.[42]

The second class of satellites, which we shall call "highly excited" satellites, possess two core holes (S $2p$ and/or S $2s$) and an excited electron, and have binding energies in

the 350–500-eV range. The excited electron is likely to be in the $6t_{1u}$ orbital, although our limited resolution does not permit confirmation of this. These states are S $2p$ and S $2s$ satellites in the sense that they could be formed from SF_6 by core-hole ionization plus excitation from a core orbital to a $6t_{1u}$ or other valence molecular orbital. These highly excited satellites are produced from *KLL-type* decay and can also be termed spectator satellites if the excited electron is in the $6t_{1u}$ level. In general, we expect that highly excited satellites with excitation energies greater than 100 eV will have negligible nonresonant intensity.

B. Resonant peak shapes and energy shifts

Conclusions about the important decay channels of SF_6^+ in the vicinity of the S $1s \rightarrow 6t_{1u}$ resonance can be drawn by examining the structure of peak *A* with reference to Table II. Off resonance (2460–2470 eV), we find that peak *A* consists of a F $1s$ peak with a binding energy of ~700 eV and a second much less intense peak with a binding energy of approximately 200 eV. This lower binding-energy peak is composed primarily of S $2p$ and S $2s$ main lines, with probable small contributions from low-excitation-energy satellites and valence peaks. At 2486 eV (on resonance), peak *A* appears as a single intense peak with a binding energy of 400(50) eV. The shape of the peak indicates very little intensity at binding energies less than 200 eV. The F $1s$ peak in Fig. 4 can be seen, partly resolved from the more intense contributions at binding energy ~400 eV. We conclude directly from the above qualitative observations that highly excited satellites produced by *KLL-type* transitions are the most im-

TABLE II. Complete description of autoionization of the $SF_6(1s^{-1}6t_{1u})$ state to SF_6^+ photoemission channels, and subsequent S(*LVV* and *LLV*) Auger cascades to form SF_6^{n+} ($n=2$–5).

	Autoionization to SF_6^+ via $1s^{-1}6t_{1u}$			Auger decay of SF_6^+ to SF_6^{n+} ($n=2$–5)		
SF_6^+ photoemission channel	Configuration[a]	Autoionization decay "type"[b]	Binding energy (eV)	Auger transitions to fill all S $2p$ and S $2s$ holes[c]	Total number of Auger electrons[d] *LLV*	*LVV*
Main lines						
$2p$	$2p^{-1}$	$KL_{2,3}V^*$	181.0[e]	$L_{2,3}VV$	0	1
$2s$	$2s^{-1}$	KL_1V^*	244.7[f]	1. L_1VV	0	1
				2. $L_1L_{2,3}V+L_{2,3}VV$	1	1
Satellites						
$2p$	$2p^{-1}\text{val}^{-1}6t_{1u}$	$KL_{2,3}V$ and	~190–220[g]	$L_{2,3}VV$	0	1
	$2p^{-1}\text{val}^{-1}v^*$	$KL_{2,3}V^*$				
$2s$	$2s^{-1}\text{val}^{-1}6t_{1u}$	KL_1V and	~255–285[g]	1. L_1VV	0	1
	$2s^{-1}\text{val}^{-1}v^*$	KL_1V^*		2. $L_1L_{2,3}V+L_{2,3}VV$	1	1
Highly excited satellites						
$2p$	$2p^{-2}6t_{1u}$	$KL_{2,3}L_{2,3}$	~360[h]	$2L_{2,3}VV$	0	2
	$2p^{-2}v^*$					
$2s$	$2s^{-2}6t_{1u}$	KL_1L_1	~490[h]	1. L_1VV+L_1VV	0	2
	$2s^{-2}v^*$			2. $L_1VV+L_1L_{2,3}V$ $+L_{2,3}VV$	1	2
				3. $L_1L_{2,3}V+L_1L_{2,3}V$ $+2L_{2,3}VV$	2	2
"Mixed"	$2p^{-1}2s^{-1}6t_{1u}$	$KL_1L_{2,3}$	~430[h]	1. $L_1VV+L_{2,3}VV$	0	2
	$2p^{-1}2s^{-1}v^*$			2. $L_1L_{2,3}V+2L_{2,3}VV$	1	2

[a]Inner- and outer-valence orbitals (binding energies 16–44 eV) are denoted by "val." Excitation due to an unoccupied molecular orbital other than $6t_{1u}$ (probably $6a_{1g}$) is denoted by "v^*."

[b]The Auger notation is used here to describe the decay *type* to the SF_6^+ photoemission final state. *V* designates that the $6t_{1u}$ electron has remained as a "spectator;" V^* denotes that the excited $6t_{1u}$ electron has participated in the decay to SF_6^+.

[c]All $2s$ holes can decay via S($L_1L_{2,3}V$) or S(L_1VV) Auger channels with some partitioning assumed independent of the configuration containing the $2s$ hole state.

[d]Auger electrons are divided into sulfur *LLV* and *LVV* categories corresponding to the two *observable* Auger peaks in our photoemission spectra. The totals here include all primary through quaternary decay to give Auger electrons within the kinetic-energy region of the two observable peaks.

[e]The S $2p$ binding energy is an average of the $2p_{3/2}$ and $2p_{1/2}$ spin-orbit binding energies which are 180.4 and 181.7 eV, respectively (Ref. 49).

[f]Reference 49.

[g]This energy range is based on observed S $2p$ satellite excitation energies (Ref. 61).

[h]Binding energy is estimated crudely by summing the binding energies (in the neutral) of the two core holes. Relaxation has not been included.

portant autoionization decay channels for the S $1s \rightarrow 6t_{1u}$ resonance.

Another indication that the photoemission channels of SF_6^+ change at the S $1s \rightarrow 6t_{1u}$ resonance energy can be found in the kinetic-energy shift of the S(LVV) and S(LLV) Auger peaks. The kinetic energies of these broad peaks are higher on resonance than off resonance. Some additional structure on the high-kinetic-energy side of the S(LVV) Auger peak also is observed on resonance. The size of the overall energy shift strongly suggests the accessibility of some new SF_6^+ states other than the S $2p$ and S $2s$ main lines. The fact that the shift is to higher kinetic energy is qualitatively rationalized below to be consistent with production of highly excited ions.

As an example, we consider the S($L_{2,3}VV$) Auger decay of SF_6^+ to SF_6^{2+} for the single-ion configurations with $2p$ holes postulated to be important off and on resonance: e.g., off resonance,

$$SF_6^+(2p^{-1}) \rightarrow SF_6^{2+}(2p^6 \mathrm{val}^{-2}) + LVV \text{ Auger } e^- ; \tag{4}$$

and on resonance,

$$SF_6^+(2p^{-2}6t_{1u}) \rightarrow SF_6^{2+}(2p^{-1}\mathrm{val}^{-2}6t_{1u}) + LVV \text{ Auger } e^- . \tag{5}$$

The kinetic energies (ε) of the S(LVV) Auger electrons in processes (4) and (5) are just the differences in energy between the ions:

$$(\varepsilon_{LVV})_{\mathrm{off}} = E(2p^{-1}) - E(2p^6\mathrm{val}^{-2}), \tag{6}$$

$$(\varepsilon_{LVV})_{\mathrm{on}} = E(2p^{-2}6t_{1u}) - E(2p^{-1}\mathrm{val}^{-2}6t_{1u}) . \tag{7}$$

The observable kinetic-energy shift ($\delta\varepsilon$) can be defined as

$$\begin{aligned}\delta\varepsilon &= (\varepsilon_{LVV})_{\mathrm{on}} - (\varepsilon_{LVV})_{\mathrm{off}} \\ &= [E(2p^{-2}6t_{1u}) - E(2p^{-1})] \\ &\quad - [E(2p^{-1}\mathrm{val}^{-2}6t_{1u}) - E(2p^6\mathrm{val}^{-2})] \\ &= [E_1] - [E_2] .\end{aligned} \tag{8}$$

The energies E_1 and E_2 both correspond superficially to the energy for promotion of a S $2p$ electron to a $6t_{1u}$ orbital, but E_1 is expected to be greater than E_2 because it requires more energy to remove a molecular core electron (i.e., $2p$) from its orbital in the presence of another core hole than in the presence of one or two diffuse holes in the valence shell, due to differences in screening. This clearly would suggest that E_1 is greater than E_2. However, the difference in the energy of the $6t_{1u}$ level in the two configurations $2p^{-2}6t_{1u}$ and $2p^{-1}\mathrm{val}^{-2}6t_{1u}$ also must be considered.[43] Because the $6t_{1u}$ orbital is least tightly bound, the dominant effect on its binding energy should be the Coulomb interaction, which is proportional to the ionic charge. Thus, the $6t_{1u}$ orbital in the $SF_6^{2+}(2p^{-1}\mathrm{val}^{-2}6t_{1u})$ configuration will experience a larger contraction than in the $SF_6^+(2p^{-2}6t_{1u})$ configuration, with the result that E_2 would be smaller than E_1. We conclude that $\delta\varepsilon$ is positive for the initial Auger decay of $2p$ hole states [processes (4) and (5)].

This positive shift for $\delta\varepsilon$ is in contrast to a shift to lower kinetic energy for Auger satellite transitions from two-hole initial states to three-hole final states.[44] However, the initial state for many Auger satellites has the second hole "exterior" to the deepest hole (e.g., KL-LLL in Ne).[45] The major effect in this case is an increased binding energy for the outer electrons which fill the core, resulting in a lower Auger kinetic energy relative to the "parent" KLL line. For Auger decay of $SF_6^+(2p^{-2}6t_{1u})$, the second $2p$ hole is in the same shell as the deepest hole, significantly affecting the screening in the core shell as well as in the valence shells.

The presence of Auger electrons from subsequent cascades to higher SF_6^{n+} ions ($n = 3$–5) significantly complicates the above discussion. Autoionization to highly excited satellites results in ions with two L-shell core holes, thus allowing for several Auger cascades. The secondary and higher Auger decay steps produce electrons with kinetic energies different from the primary Auger electron due to core and valence screening differences and the degree of involvement of the excited $6t_{1u}$ electron. The additional structure in the S(LVV) Auger peak may arise from such effects. Further explanation of these issues will be warranted when higher-resolution spectra become available.

As further support for the importance of the resonant SF_6^+ highly excited satellite channels and subsequent Auger cascades, we can compare the S(LVV) Auger peak observed at the S $1s \rightarrow 6t_{1u}$ resonance with the S(LVV) peak observed above the S $1s$ threshold. We find that the S(LVV) peak shapes are very similar in these two cases. The primary contributions to the S(LVV) peak above the S $1s$ threshold (see Table I) must be from secondary and higher-order Auger decay following S $1s$ ionization, because sulfur K-shell ionization is stronger at these energies than the sulfur L-shell ionization processes. Furthermore, the initial Auger decay of the S $1s$ hole will be mostly KLL because the S $2p$ and S $2s$ orbitals (more than F $1s$ and valence) reside on the sulfur atom, providing good overlap with the S $1s$ orbital. This result for the initial decay step also can be deduced by comparison with Ar,[46] and shows that higher-order Auger decay from SF_6^{2+} starts primarily from configurations with two holes in the sulfur L shell ($2p^{-2}$, $2s^{-1}2p^{-1}$, and $2s^{-2}$). Still another way to reach the same conclusion is to note that KLL decay is the principle deexcitation process in light elements. The similarity of the S(LVV) peaks above and below threshold indicates that configurations with two L-shell holes (e.g., $2p^{-2}6t_{1u}$) probably provide important decay channels for the S $1s \rightarrow 6t_{1u}$ resonance.

C. Sulfur $I(LVV)/I(LLV)$ Auger intensity ratio

The qualitative assertion that highly excited satellites dominate the decay of the $1s^{-1}6t_{1u}$ state can be documented further using the observable sulfur Auger intensity ratio $I(LVV)/I(LLV)$.[47] Experimentally, the $I(LVV)/I(LLV)$ intensity ratio changes from 3.0(3) off resonance to 25(5) at 2486 eV (Fig. 6). The enhancement in the Auger intensity ratio depends directly on the relative resonant cross sections for the highly excited satellite states. In fact, careful examination of the contributions to

the observable Auger ratio leads to the identification of the most important highly excited satellite channel.

We shall now show that it is possible to express the $I(LVV)/I(LLV)$ Auger ratio in terms of the dominant SF_6^+ cross sections provided that all subsequent Auger decay steps are accounted for. Columns 5–7 of Table II outline the primary through quaternary decay steps to form SF_6^{n+} ($n=2$–5) for each photoemission channel. For this estimate, we first assume that the ions Auger decay quickly enough to fill all core holes (S $2p$ and S $2s$) before dissociation can occur. A comparison of SF_6 ground-state vibrational lifetimes ($\sim 5\times10^{-14}$ sec, Ref. 48) with S $2p$ and S $2s$ core-hole lifetimes (5×10^{-15} and 1.4×10^{-15} sec, respectively)[49] indicates that Auger decay of these holes is probably at least ten times faster than the dissociation rate. If infrequent dissociation does occur, leaving an ion fragment SF_n^+ ($n<6$) with a sulfur L hole, the fragment itself will Auger decay to fill the core hole. Thus, the issue of dissociation does not significantly affect the following analysis of the S(LLV) and S(LVV) Auger peaks.

An additional factor necessary for deriving the $I(LVV)/I(LLV)$ ratio is the fraction of S $2s$ holes which decays via the Coster-Kronig S($L_1L_{2,3}V$) Auger pathway

$$SF_6^+(2s^{-1}) \rightarrow SF_6^{2+}(2s^2 2p^{-1}\mathrm{val}^{-1}) + L_1L_{2,3}V \text{ Auger } e^-, \tag{9}$$

rather than the S(L_1VV) pathway

$$SF_6^+(2s^{-1}) \rightarrow SF_6^{2+}(2s^2\mathrm{val}^{-2}) + L_1VV \text{ Auger } e^- . \tag{10}$$

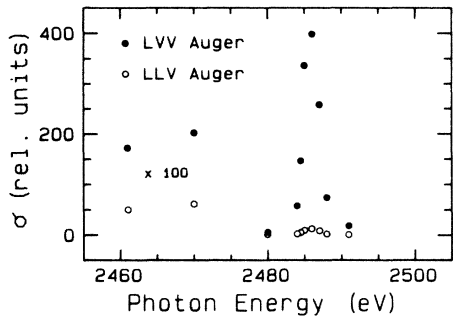

FIG. 6. Relative cross sections for the S($L_{1,2,3}VV$) and S($L_1L_{2,3}V$) Auger electrons over the S $1s\rightarrow 6t_{1u}$ resonance. The scale for the two lowest-energy points has been expanded 100 times.

In our analysis, we have assumed that this partitioning into the S($L_1L_{2,3}V$) and S(L_1VV) Auger-decay pathways is *independent* of the configuration containing the S $2s$ hole. For example, the fraction f of S $2s$ holes decaying via the Coster-Kronig S($L_1L_{2,3}V$) channel is assumed to be the same for the configurations $SF_6^+(2s^{-1})$ and $SF_6^+(2s^{-2}6t_{1u})$. The presence of these two possible Auger-decay channels is evident in column 5 of Table II for each SF_6^+ state containing a S $2s$ hole.

The intensity ratio $I(LVV)/I(LLV)$ in general (on and off resonance) can be derived in terms of f by adding up all the singly charged ion cross sections which can subsequently Auger decay via LVV and LLV pathways as

$$\frac{I(LVV)}{I(LLV)} = \frac{1}{f}\,\frac{\sigma(2p)+\sigma(2p\ \mathrm{sat})+\sigma(2s)+\sigma(2s\ \mathrm{sat})+2[\sigma(2p^{-2}v^*)+\sigma(2s^{-2}v^*)+\sigma(2p^{-1}2s^{-1}v^*)]}{\sigma(2s)+\sigma(2s\ \mathrm{sat})+\sigma(2p^{-1}2s^{-1}v^*)+2\sigma(2s^{-2}v^*)}, \tag{11}$$

where $\sigma(x)$ represents the cross section for the SF_6^+ photoemission channel x.

The fraction f can be determined from the nonresonant Auger ratio and the $\sigma(2p)/\sigma(2s)$ cross-section ratio. Away from the S $1s\rightarrow 6t_{1u}$ resonance ($h\nu<2480$ eV), the expression for the $I(LVV)/I(LLV)$ ratio can be simplified with the assumption that the S $2s$ and S $2p$ main lines are the only SF_6^+ channels which contribute to the S(LVV) and S(LLV) Auger peaks. With all satellite cross sections assumed negligible, the nonresonant ratio becomes

$$\left[\frac{I(LVV)}{I(LLV)}\right]_{\mathrm{off}} = \frac{1}{f}\,\frac{\sigma(2s)+\sigma(2p)}{\sigma(2s)} = \frac{1}{f}\left[1+\frac{\sigma(2p)}{\sigma(2s)}\right]. \tag{12}$$

The $\sigma(2p)/\sigma(2s)$ cross-section ratio in Eq. (12) can best be estimated from measurements of this ratio in atoms excited with high-energy x-ray sources. From these trends in low-Z elements, we expect that for sulfur, the $\sigma(2s)/\sigma(2p)$ ratio should be between 1.0 and 3.0.[49] This assumption leads ultimately to a value of f greater than 0.4. This crude result can be compared to the Ar $L_1L_{2,3}M$ and L_1MM Auger intensities which show that the Coster-Kronig channel in Eq. (9) is the overwhelmingly favored decay pathway for an Ar $2s$ hole.[50] The fraction f for Ar has been determined from experiment and theory to be greater than 0.95.[50]

Considering Eq. (11) for the resonant $I(LVV)/I(LLV)$ ratio, we use the assertion from Sec. IV B that the highly excited satellite channels dominate the decay of the S $1s\rightarrow 6t_{1u}$ resonance to simplify the expression for the $I(LVV)/I(LLV)$ Auger ratio:

$$\left[\frac{I(LVV)}{I(LLV)}\right]_{\mathrm{on}} = \frac{2}{f}\left[\frac{\sigma(2p^{-2}v^*)+\sigma(2s^{-2}v^*)+\sigma(2p^{-1}2s^{-1}v^*)}{\sigma(2p^{-1}2s^{-1}v^*)+2\sigma(2s^{-2}v^*)}\right] = \frac{2}{f}\left[\frac{\sigma_{\mathrm{tot}}}{\sigma(2p^{-1}2s^{-1}v^*)+2\sigma(2s^{-2}v^*)}\right]. \tag{13}$$

It is clear upon inspection of Eq. (13) that in order for

$[I(LVV)/I(LLV)]_{on}$ to be as large as the observed ratio on resonance (25±5), the cross sections $\sigma(2s^{-2}v^*)$ and $\sigma(2p^{-1}2s^{-1}v^*)$ must be relatively small. In fact, the expression in large parentheses on the right-hand side of Eq. (13) must lie in the range 4—15 (using $0.4 \leq f \leq 1.0$). Even with this large uncertainty, these values indicate that at least 75% of the S $1s \rightarrow 6t_{1u}$ resonant cross section appears in the $2p^{-2}v^*$ channel.

The dominance of the resonant $SF_6^+(2p^{-2}v^*)$ channel is not surprising if one examines the expected partitioning of the cross sections within an Auger-like decay scheme. In other words, if the $6t_{1u}$ electron is left always as a spectator, we can consider the core decay to be much like normal K-hole Auger decay. The KLL-type decay channels (highly excited satellites) should then dominate over the $KLV(V^*)$ decay pathways (main lines and low-excitation-energy satellites), which is observed qualitatively in our analysis of peak A on resonance. Furthermore, the partitioning into the three important KLL-type channels can be compared with three schemes: (1) statistical, (2) Ar KLL Auger decay,[46,51] and (3) SF_6 S(KLL) Auger decay.[52] The partitioning in these scenarios is shown in Table III. It is clear that an Auger-*like* decay mechanism (similar to Ar and SF_6 KLL Auger rates) with dominant decay to the $2p^{-2}6t_{1u}$ state is consistent with our interpretation of the $I(LVV)/I(LLV)$ ratio on resonance, within the assumptions made.

In summary, the $1s^{-1}6t_{1u}$ resonant state decays predominantly to the highly excited satellite configurations of SF_6^+ ($2p^{-2}v^*$, $2p^{-1}2s^{-1}v^*$, and $2s^{-2}v^*$). The decay of the excited state is such that the $6t_{1u}$ electron (v^*) probably remains as a spectator, and the S $1s$ hole decays in a manner similar to Ar and SF_6 KLL Auger decay. Consistent with this, we find that at least 75% of the resonant cross section appears in the $SF_6^+(2p^{-2}v^*)$ channel.

D. Resonant asymmetry parameters

The asymmetry parameters for the S(LVV) peak and peak A provide additional information on the photoemission and subsequent Auger-decay channels at the S $1s \rightarrow 6t_{1u}$ resonance. Figure 7 shows β values for the S(LVV) Auger peak and peak A, both demonstrating marked changes on resonance. We note that the behavior of the β(peak A) mostly is due to the photon-energy-dependent changes in the cross sections of the unresolved components of peak A. Below the S $1s \rightarrow 6t_{1u}$ resonance, about 85% of the peak-A intensity is F $1s$ photoemission, yielding β near 2.0. On resonance, the F $1s$ cross section remains unaltered while the other components of peak A exhibit a large increase in cross section, as seen in Fig. 4. The dominance of the S $2p$ and S $2s$ highly excited spectator-satellite cross sections causes the β(peak A) to mimic the β value for these resonant levels, which appears to be near zero or slightly negative on resonance. The presence of unresolved contributions (spectator satellites) in peak A prohibits the measurement of the individual-channel asymmetry parameters.

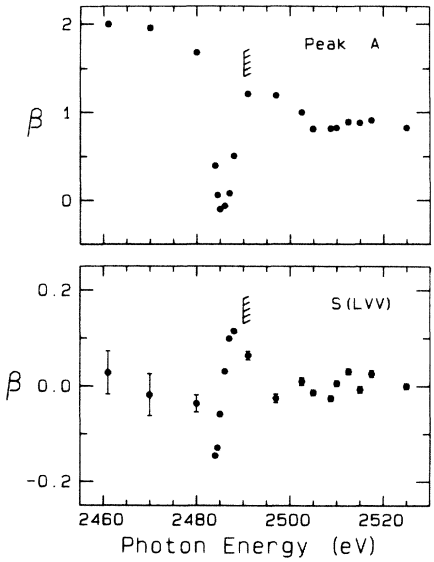

FIG. 7. Angular-distribution parameters for peak A (top) and S(LVV) Auger (bottom) over the S $1s \rightarrow 6t_{1u}$ resonance. The oscillations in β(peak A) above the S $1s$ threshold mainly are caused by added contributions from S(KLL, KLV, and KVV) Auger electrons.

Unlike the oscillations in β(peak A), the asymmetric profile for the $\beta(LVV)$ at the S $1s \rightarrow 6t_{1u}$ resonance cannot be dismissed as arising from variations in peak-component cross sections. Although the oscillation is small (±0.12) and more data on the wings of the resonance are needed to confirm the exact shape, the $\beta(LVV)$ clearly is affected. In addition, the maximum in σ(peak A) in Fig. 5, $\sigma(LVV)$ and $\sigma(LLV)$ in Fig. 6, and the minimum in β(peak A) in Fig. 7 all lie at 2486.0(5) eV, the energy at which the $\beta(LVV)$ crosses its background value, further confirming the asymmetric shape. This result for an *Auger* angular distribution is particularly intriguing because no previous studies have reported angle-resolved Auger decay emanating from ions resonantly produced by autoionization below a deep core-level threshold. Even though this unusual resonant profile for an Auger β should be considered tentative, some implications of an asymmetric shape are worthy of discussion.

An asymmetric profile in β ordinarily signals an interference effect. However, the interference in the autoionization process occurs one step previous to the observed Auger decay. That is, the direct-ionization and excited-state autoionization pathways leading to SF_6^+ in-

TABLE III. Relative intensities for the highly excited satellite channels for the S $1s \rightarrow 6t_{1u}$ resonance in SF_6 compared to KLL Auger decay.

Scheme	Relative intensity $2p^{-2}$	$2s^{-1}2p^{-1}$	$2s^{-2}$
1. Statistical decay	0.54	0.43	0.04
2. Ar KLL-like decay[a]	0.74(5)	0.22(5)	0.04(1)
3. SF_6 S(KLL)-like decay[b]	0.72(1)	0.21(2)	0.07(3)
4. Observed decay	>0.75		

[a]References 46 and 51.
[b]Reference 52.

terfere, causing oscillations in the σ and β values for the single-ion channels. Subsequent Auger decay cannot experience this interference phenomenon directly, but may retain "memory" of the process due to ion alignment.

Following up the idea of ion alignment, the Auger electron β is, in a sense, a "snapshot" of the molecular orientation of the SF_6^+ ion prior to Auger decay. According to Dehmer and Dill's formalism, β_{Auger} can be expressed as[27]

$$\beta_{\text{Auger}}=c\beta_m\ , \tag{14}$$

where c is a constant characteristic of each individual Auger-decay channel, and β_m is the asymmetry of the molecular *ion* orientation following photoionization. Because autoionization to $2p^{-2}v^*$ dominates the S $1s\rightarrow 6t_{1u}$ resonance, the oscillation in $\beta(LVV)$ should reflect primarily the orientation of this particular SF_6^+ ion configuration in the resonance region. A varying energy dependence of single-ion alignment due to autoionization has been observed previously in atomic Cd for the double excitations above the $4d$ threshold [$4d^9(5s\,5p^3P)6s\,^1P$, Ref. 53] and over the $4d\rightarrow np$ ($n\geq 8$) and nf ($n\geq 5$) Rydberg series.[54]

A remaining point to consider is the relationship between the molecular-ion asymmetry β_m and the resonant photoelectron asymmetry parameter for the major channel $2p^{-2}v^*$. The asymmetry in the alignment of the $2p^{-2}v^*$ ion suggested by the S(LVV) β results also should appear in the β of the $2p^{-2}v^*$ photoelectron, which is convoluted in the total β(peak A). However, the individual profile cannot be determined from the β(peak A) because of the unresolved components and the rapidly changing cross sections.

To summarize, the asymmetric profile for the S(LVV) Auger β over the S $1s\rightarrow 6t_{1u}$ resonance, though tentative, is highly unusual. Though the conceptual link between the Auger-electron β and single-ion alignment is provided by Dehmer and Dill's theory,[27] there are no available calculations for the specific shape of the molecular orientation asymmetry β_m over a discrete resonance.

V. ABOVE THE S 1s THRESHOLD

For the data taken above the sulfur K edge, both σ(peak A) and $\sigma(LVV)$ cross sections (Fig. 5) show characteristic undulations in the S $1s$ continuum. In particular, the peak near 2507 eV is evident in our data (the unresolved d and e features in Fig. 1), as are broader features at ~2525 and 2555 eV (f and g in Fig. 1). Oscillations also appear in σ(S $1s$) and β(S $1s$) shown in Fig. 8. For the sake of illustration, the σ(S $1s$) data for SF_6 have been normalized to the absorption curve.[1] The MSM-$X\alpha$ σ(S $1s$) and β(S $1s$) are also shown.[13]

The S $1s$ continuum results will be discussed in two parts. In Sec. V A we examine our data near the 2507-eV resonances and interpret sharp changes in the cross-section ratios σ(peak A)/$\sigma(1s)$ and $\sigma(LVV)/\sigma(1s)$ as indications of resonant enhancement in the S $2p$, S $2s$, and valence main-line and satellite channels. This behavior and the observation of S $1s$ satellites lead to an assignment of the two resonances visible in the photoabsorption

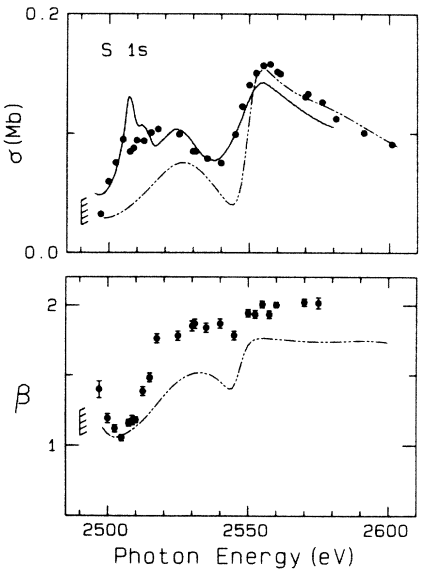

FIG. 8. S $1s$ partial cross section (top) and asymmetry parameter (bottom) plotted with MSM results (dashed curve) (Ref. 13). The solid curve is the photoabsorption measurement (Ref. 1) with the below-threshold nonresonant contributions subtracted. The cross-section data have been scaled to this adjusted absorption curve at 2535 eV.

cross section at 2506 and 2511 (d and e) as doubly excited states.

Section V B will address the nature of the features at 2525 and 2555 eV photon energy. We compare the experimental data with a single-scattering plane-wave EXAFS calculation and with MSM-$X\alpha$ results. This is followed by a discussion in terms of approximations to the electron-scattering process and the description of the molecular potential in EXAFS and MSM-$X\alpha$ calculations which attempt to model the effects in this energy region.

A. The 2507-eV resonances and S 1s satellites

The σ(S $1s$) data in Fig. 8, in contrast to $\sigma(LVV)$ and σ(peak A) cross sections in Fig. 5, do not show a sharp feature at 2507 eV. To illustrate the differing behavior at this resonance, the cross-section ratios σ(peak A)/σ(S $1s$) and $\sigma(LVV)/\sigma$(S $1s$) are plotted in Fig. 9. In the ratio plots, the behavior at 2507 eV is much more pronounced. This peak appears as one resonance in Fig. 9 and is 4—5 eV full width at half maximum. Both the 2506 and 2511 eV resonances discernable in the photoabsorption measurement[1] (see Fig. 1, d and e) probably are present in our lower-resolution results. Because of the contributions included in the measured peaks (see Table I), we stress that any sharp changes in the ratios below the S $1s$ satellite thresholds are due to resonant contributions of the S $2p$, S $2s$, and valence main lines and satellites (low-excitation and highly excited satellites). Furthermore, the peak at 2506 eV and its shoulder at 2511 eV in the photoabsorption curve do not appear in the MSM-$X\alpha$ theory curve, indicating that they probably are caused by a multielectron resonance or a symmetry-forbidden process.

The β(S $1s$) in Fig. 8 also shows a dramatic effect in this low-energy region. The β falls from 2 at high photon

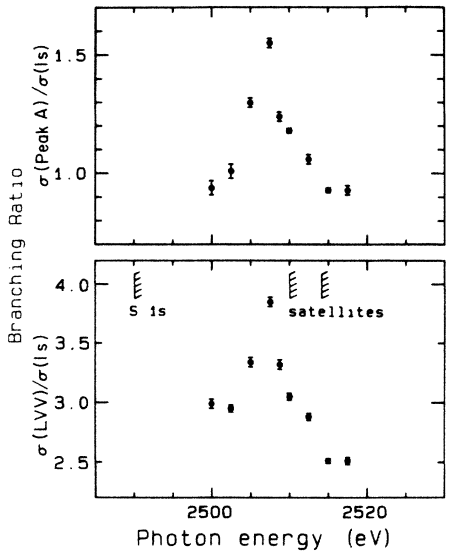

FIG. 9. Cross-section ratios σ(peak A)/σ(S 1s) (top) and $\sigma(LVV)/\sigma$(S 1s) (bottom) in the vicinity of the 2507-eV resonances. For the ratio σ(peak A)/σ(S 1s), the F 1s cross section has been subtracted from the peak-A intensity using the F(KVV) Auger intensity in each spectrum. Observed S 1s satellite and main-line thresholds also are shown.

energy to a minimum at 2507 eV of 1.1. The MSM calculation shows a decrease in β(S 1s) in this region, even though it does not predict the photoabsorption features at 2506 and 2511 eV. Thus, it is not clear from comparison with theory whether the β(S 1s) effect is associated with the 2507-eV feature. The departure of β(S 1s) from the atomic value of 2.0 for an s orbital is a direct indication of the anisotropy of the molecular potential.

Pertinent to this resonance region, two S 1s correlation satellite peaks were observed directly at higher photon energies. Figure 3 shows the satellites at a representative photon energy of 2581 eV. We report an average branching ratio for the total satellite intensity relative to the S 1s main line of 15(3)% in the photon-energy range between 2570 and 2590 eV. The satellite thresholds were measured from a series of spectra to be 2510(1) and 2514(1) eV, 20 and 24 eV above the S 1s threshold, respectively. Note that the satellite binding energies are located 3—4 eV above the 2506- and 2511-eV photoabsorption features (d and e).

The observed satellite binding energies, combined with the sharp changes in the cross-section ratios discussed above, present a strong case for assignment of the resonant features as doubly excited autoionization states preceding the satellite thresholds. The general assignment of features d and e as multiple excitations has been suggested previously.[4] The possible decay channels of the postulated doubly excited resonances are depicted in Fig. 2 (dotted lines). The two resonances somewhat resolved in the absorption measurement may be leading to the two observed satellite thresholds. In analogy to the S $1s\rightarrow 6t_{1u}$ resonance, the configurations for the neutral doubly excited states could be $1s^{-1}(\text{val})^{-1}v^{*}6t_{1u}$, leading to the satellite ionic states $1s^{-1}(\text{val})^{-1}v^{*}$ of SF_6^{+}. The $6t_{1u}$ electron is included in the excited-neutral configuration because the energy spacing of the resonance below the satellite thresholds (3—4 eV) is similar to the spacing of the S $1s\rightarrow 6t_{1u}$ transition below the S 1s edge. However, multiplet splitting of the resonant states can be significant and will complicate the details of this simple assignment.

The intensity of these doubly excited resonances seems reasonable by comparison to the S $1s\rightarrow 6t_{1u}$ resonant intensity. The increase in the total cross section at one of the doubly excited resonances is about 3(1)% of the increase at the S $1s\rightarrow 6t_{1u}$ resonance, while the total photoemission intensity of the S 1s satellites relative to the S 1s main line photoemission is approximately 15%.

There have been no calculations to help identify the possible S 1s satellite configurations. Therefore, using the current valence ordering of Dehmer *et al.*[20] and the $4t_{1u}\rightarrow 6a_{1g}$ transition energy of $\sim$17 eV in the neutral molecule,[20] we crudely approximated the possible shake-up and conjugate shake-up satellites in the energy region of interest.[55] We have considered only promotion of an outer-valence electron to the $6a_{1g}$ and $6t_{1u}$ unoccupied orbitals. Based on energetics alone, this approach indicates that the observed S 1s satellites have the possible SF_6^{+} configurations

$$1s^{-1}(5a_{1g})^{-1}6a_{1g},$$

$$1s^{-1}(4t_{1u})^{-1}6t_{1u},$$

$$1s^{-1}(5a_{1g})^{-1}6t_{1u}\ \text{(conjugate shake-up)},$$

though the conjugate shake-up state seems less likely. These configurations correspond to excitation from the deepest outer-valence orbitals.

The general identification of these resonances as doubly excited states is reasonably clear, but in disagreement with the earlier assignment of one of them (2506 eV, feature d) as a symmetry-forbidden shape resonance.[3] Detailed theoretical calculations are needed to determine the energy positions of both the autoionization states and satellite thresholds, and the intensity effects at the resonances.

B. High-energy features

For the two higher-energy maxima at about 2525 and 2555 eV in σ(S 1s), there is good agreement with the MSM calculation (Fig. 8). The S 1s kinetic energies at these maxima are about 35 and 65 eV, respectively. The magnitude of the increase in the experimental S 1s cross section near 2555 eV is quite large, about a factor of 2 over an energy range of 15 eV. The cross-section effect is probably accentuated by the suppression of the continuum intensity related to the huge enhancement of the S $1s\rightarrow 6t_{1u}$ discrete resonance.

The significant scatter and uncertainty in the β(S 1s) measurements above 2530 eV preclude any strong statements about an effect in the angular distribution associated with the rise in the cross section around 2545 eV. The MSM curve shows a minimum in β(S 1s) which coincides with the S 1s cross-section minimum.

Because of the agreement between the MSM and experimental cross sections, we further consider the general

MSM results for SF_6. The nature of these high-kinetic-energy oscillations was mentioned briefly by Wallace as originating from EXAFS behavior.[13] The MSM theory to some extent includes all single- and multiple-scattering events in the calculation of partial cross sections, so the particular physical effect(s) producing the oscillations is not clear when only cross-section results are available. Wallace noted that there are no calculated symmetry-allowed shape-resonant states in this energy region; the presence of such quasibound states would be unusual considering the required barrier height ($\gtrsim$35 and 65 eV) needed for trapping the photoelectron. However, the eigenphase sum for S $1s(1a_{1g})\rightarrow\varepsilon t_{1u}$ photoionization rises by $\sim\pi/3$ over an energy range of 15 eV centered at $\sim$2549 eV photon energy,[56] which is the center of the rise in the S 1s cross section. There is also a marked similarity among the calculated MSM cross sections for the various core levels of SF_6 in this kinetic-energy range. We will not elaborate on this similarity except to note that the intensity changes around 60 eV kinetic energy may be caused by a single phenomenon.

Because Wallace[13] interpreted the high-energy features as EXAFS, we have performed a single-scattering plane-wave EXAFS calculation for comparison with experiment to help determine the physical origin of these features by identifying the EXAFS portion of the continuum oscillations. The factors of short bond distance ($r=1.58$ Å) and strong backscattering amplitude which make single-scattering EXAFS pronounced are indeed present in SF_6. The calculated EXAFS oscillatory amplitudes using a Debye-Waller factor of $\sigma=0$ (best case for large amplitudes) and two different central-atom phase shifts (sulfur and "adjusted" phase shifts) are shown in Fig. 10, plotted with the absorption curve (where the below-threshold nonresonant intensity has been subtracted) and the MSM-$X\alpha$ S 1s partial cross section. For the F backscattering atoms, the published Clementi-Roetti phase shifts and amplitudes were used.[57,58] Various central-atom phase shifts other than those for sulfur were tried until the calculated high-kinetic-energy oscillations coincided with the experimental energies of approximately 140, 215, and 295 eV (see Fig. 10, vertical lines). The resulting adjusted central-atom phase shift corresponds to a curve between that for Na and Mg (the Clementi-Roetti $l=1$ phase shifts with the $Z+1$ approximation); quantitatively, this equals the Si phase shift minus a value of 1.25 rad.[57] Though the variation of the central-atom phase shift did serve to line up the high-kinetic-energy EXAFS features, it also reduced the effect in the cross section by a factor of 2. For this reason, we also show in Fig. 10 the calculated EXAFS curve using the unadjusted sulfur phase shifts (dashed curve, bottom).

A comparison between the calculated EXAFS curve (with adjusted phase shifts) and experiment shows good agreement above $\sim$120 eV kinetic energy in the amplitude of the EXAFS oscillations when an estimated background cross section is used (see top of Fig. 10, dotted line). The features below 100 eV, however, are not as well reproduced. It is difficult to assess the relative intensity effect for SF_6 in this region because of the uncertainty in the nondiffractive experimental "background," though we can

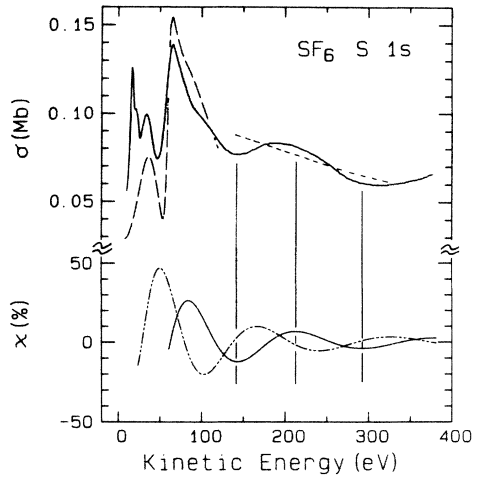

FIG. 10. S 1s scattering plane-wave EXAFS oscillatory amplitudes χ (%) for SF_6 as a function of kinetic energy (bottom). The solid and dashed curves represent the χ (%) calculated with the adjusted and sulfur central-atom phase shifts, respectively. The photoabsorption curve (Ref. 1) is plotted on an absolute scale for comparison (solid curve, top), along with the MSM-$X\alpha$ S 1s partial cross section (Ref. 13) (dot-dashed curve, top). The "non-EXAFS" background cross section has not been subtracted from the experimental absorption data. Above 100 eV kinetic energy, an estimation of the sloping background can be made (dashed curve, top) for comparison of the amplitude effects for that energy range. The vertical lines are drawn to emphasize the energy agreement between the adjusted phase-shift EXAFS calculation and the experimental absorption data.

set a *lower* limit on the effect in the S 1s cross section at about 50%. The EXAFS calculation with the adjusted phase shift shows a 25% effect in this energy region, while the EXAFS curve using the sulfur-atom phase shift shows a 50% effect. We believe that the uncertainties in both the experimental and calculated amplitudes below 100 eV kinetic energy do not permit any conclusions based on intensity arguments.

Using the adjusted phase shifts to reproduce the energies of the high-kinetic-energy wiggles, the maximum of the large peak at 65 eV kinetic energy is off by $\sim$20 eV in energy. This particularly poor energy agreement is reinforced when similar calculations on Br_2 and $GeCl_4$ are examined. The calculations for these molecules reproduce the corresponding experimental energies at both high energies *and* between 4 and 5 Å^{-1} (60–100 eV).[58] It is known that atoms less electronegative than fluorine are not as effective in creating a barrier in the molecular potential which can modify the atomic effects.[3] These facts point to the possible importance of molecular effects in SF_6. Considering all of these factors, we conclude that the cross-section features at 35 and 65 kinetic energy in SF_6 (f and g in Fig. 1) do not arise exclusively from a simple single-scattering plane-wave EXAFS phenomenon.

Summarizing the results to this point, our conclusions are that the MSM-$X\alpha$ calculation[13] reproduces the experimental S 1s cross section well below 100 eV kinetic energy (Fig. 10, top, dot-dashed curve), whereas our single-

scattering plane-wave EXAFS calculation does not. The next question is how to improve the general theoretical treatment of this problem. Two types of "fine-tuning" of the theory involve first, a better description of the electron-scattering process, and second, improvement in the treatment of the molecular potential. These two improvements are not necessarily separate developments.

EXAFS theorists recently have been interested in improving the description of the scattering process by introducing spherical waves into the single-scattering calculations.[28–31] One can make an intuitive argument that the curvature of the wave front will be more important at low kinetic energies and for molecules with short bond distances.[31] From a more quantitative point of view, Lee and Pendry have done plane- and spherical-wave calculations on crystalline Cu.[28] The spherical-wave corrections to the Cu EXAFS curve shift the oscillations by an energy on the order of 20 eV and reduce the amplitude by a factor of 2 below 100 eV. Based on these crude estimates, we think that curved-wave-front corrections (which we have neglected in our calculation) should be important for SF_6 in the kinetic-energy range below 100 eV, affecting both the amplitude and phase of the EXAFS features.

The complication of multiple-scattering events should also be considered in this energy range (MSM theory of course includes these events). Multiple-scattering contributions to EXAFS have been calculated on a variety of systems with the following trends having been exhibited. First, the most important effect occurs with an arrangement of collinear atoms where the intervening atom serves to "focus" amplitude back onto the central atoms.[33–35] This focusing effect usually involves only one backscattering event and can result in a significantly enhanced amplitude and a phase shift at all energies.[33] A similar multiple-scattering path for SF_6 can be denoted S-F_1-S-F_2-S, where F_1 and F_2 are fluorine atoms collinear with the sulfur atom. Secondly, large-angle scattering can be significant, especially at low energy where electron scattering becomes more isotropic. Bunker and Stern[35] estimated that below 30 eV kinetic energy for Mn 1s ionization of $KMnO_4$, the large-angle multiple-scattering amplitude relative to single scattering is about 25–50% (and about 10–20% at higher energy).

However, even with spherical-wave and multiple-scattering corrections included which improve the treatment of the electron scattering process, there may still be significant interaction with the more diffuse molecular potential below 100 eV kinetic energy. A recent experimental study on the oxygen K-edge EXAFS spectra of O_2, CO, and CO_2 concludes that the observed disagreement between these experiments and single-scattering EXAFS theory is probably caused by inappropriate atomic parameters in the EXAFS calculation.[59] The atomic parameters and potential were thought to be inaccurate for modeling the electron scattering in the molecular orbitals.[59] The current degree of modification of EXAFS theory fails to include the complicated electronic structure and interaction due to the *molecular* nature of the problem. For example, in the atomic phase-shift EXAFS calculations of Lee and Beni,[60] two atomic muffin-tin potentials are calculated separately and overlapped. Of course, the details of the potential between the atoms are not muffin-tin-like, as the authors note. The inaccuracies in this region should not affect the EXAFS calculations at high-energy because any complexity will not be experienced by a high-energy electron. It is exactly in this region, however, where low-energy electrons may interact more with the details of the molecular potential.

MSM-$X\alpha$ calculations use as a starting point atomic potentials similar to those used in EXAFS theory.[13,15] The molecular detail between the atoms is picked up, albeit indirectly, by a self-consistent treatment of the molecular potential. The possible nature of the interaction with the molecular field above approximately 30 eV kinetic energy has not been considered previously. The same interaction at lower kinetic energy can result in shape resonances, which are reasonably well understood. However, even in this respect SF_6 seems to be an especially complicated case.[19,20,61]

In order to qualitatively imagine how a high-energy (30–60 eV kinetic energy) interaction might occur, it is useful to think of the simple square-barrier potential problem where[62]

$$\begin{aligned} &V = V_0, \quad 0 \le r \le r_0 \\ &V = 0, \quad r < 0 \text{ and } r > r_0 \ . \end{aligned} \tag{15}$$

When the energy of a wave is greater than the barrier height V_0, the wave is quantum-mechanically transmitted *and* reflected, giving oscillations in the continuum cross section, frequently called transmission resonances. The largest effect occurs with a large barrier width and/or height. Certainly, the realistic addition of a potential well and a repulsive wall may perturb even the qualitative aspects of this effect, but we use this simple example to illustrate the possible nature of an interaction between the photoelectron and a possibly large barrier induced by the electronegative fluorines in SF_6.

We believe that the future understanding of this phenomenon will come primarily from detailed theoretical work which examines the origins of the dipole matrix-element changes in this energy range. The results of a step-by-step EXAFS calculation for SF_6, where spherical-wave and multiple-scattering corrections are added sequentially, would certainly help to estimate the importance of interaction with the atomic cores (EXAFS) relative to that with the more diffuse aspects of the molecular potential. Improvements in the potential itself are necessary also to pick up the possible nondiffractive (barrier) interactions that occur in this intermediate-energy range. Combined with this, a careful examination of the results of the MSM-$X\alpha$ calculation, which quantitatively reproduces the cross section between 25 and 100 eV kinetic energy, could yield some insight into the physical origin(s) of these high-energy features.

VI. CONCLUSIONS

To summarize, the specific conclusions which can be drawn from our data near the sulfur K edge in SF_6 are as follows.

(1) For the S 1s $(1a_{1g}) \rightarrow 6t_{1u}$ resonance, highly excited

satellites with *two* core holes (S 2*p*, S 2*s*) are the important SF_6^+ decay channels. These configurations ($2p^{-2}v^*$, $2s^{-2}v^*$, and $2p^{-1}2s^{-1}v^*$), if regarded as S 2*s* and S 2*p* satellites, have exceptionally high excitation energies (>150 eV) and, according to the spectator model, probably contain a $6t_{1u}$ electron in the excited v^* orbital. In general, our data suggest that the decay of the neutral excited state proceeds much like Ar *KLL* and SF_6 S(*KLL*) Auger decay, with the $2p^{-2}v^*$ channel as the dominant one. Furthermore, an asymmetric resonant profile for the S(*LVV*) Auger β is observed, probably caused by ion alignment in the previous photoemission step.

(2) The resonances around 2507 eV are probably doubly excited autoionizing states (leading to observed satellite thresholds), because decay into S 2*p*, S 2*s*, and/or valence photoemission channels is observed. The interpretation emphasizes the general requirement for results on individual photoemission channels in order to distinguish satellite continua and autoionization effects from shape resonances in the assignment of absorption features.

(3) The data further above the S 1*s* threshold (30–100 eV kinetic energy) are difficult to interpret. The experimental results show a factor-of-2 increase in the S 1*s* cross section near 2550 eV, but no conclusive effect in the S 1*s* β. MSM-$X\alpha$ calculations successfully reproduce the effect in the S 1*s* cross section, indicating their one-electron nature.[13] We conjecture that the large effects are caused by a combination of spherical-wave and multiple-scattering effects in EXAFS and an interaction of the photoelectron with the details of the molecular potential.

There is an obvious need for further experimental work in several areas. High kinetic-energy resolution would help to assign the SF_6^+ resonant states (i.e., the location of the excited electron) and possibly the structure of the broad sulfur *LLV* and *LVV* Auger peaks on and off resonance. The decay of core-level discrete states in molecules has been examined in just a few systems to date.[22–26,61,63–65] We predict that future resonant work below deep core-level thresholds will confirm the predominance of highly excited satellites and the importance of spectator decay. The study of core levels of other octahedral molecules with electronegative ligands and of substituted hexafluorides (like SF_5X) with respect to the continuum effects above 30 eV kinetic energy may help to determine the origin of the cross-section effects in this energy region.

On the theory side, resonance calculations are needed for individual cross sections and angular distributions. More general work on the theory for Auger-electron angular distributions is called for to elucidate how autoionization produces an aligned molecular ion prior to Auger decay. Finally, advances in EXAFS theory as applied to molecules, especially concerning the treatment of the electron-scattering process and of the molecular potential, are needed to investigate the nature of interactions with low-energy (<100 eV) electrons.

ACKNOWLEDGMENTS

We would like to acknowledge Z. Hussain for assistance with the experimental preparations and discussions with J. L. Dehmer, J. A. Stephens, J. J. Barton, and M. N. Piancastelli. This work was supported by the Director, Office of Energy Research, Office of Basic Energy Sciences, Chemical Sciences Division of the U.S. Department of Energy under Contract No. DE-AC03-76SF00098. It was performed at the Stanford Synchrotron Radiation Laboratory, which is supported by the Department of Energy's Office of Basic Energy Sciences.

*Permanent address: Technische Universität Berlin, Institut für Strahlungs-und Kernphysik, Sekr. PN 3-2, Hardenbergstr. 36, D-1000 Berlin 12, West Germany.

[1]R. E. LaVilla and R. D. Deslattes, J. Chem. Phys. **44**, 4399 (1966).

[2]T. M. Zimkina and A. S. Vinogradov, J. Phys. (Paris) Colloq. **32**, C4-3 (1971), and references therein.

[3]J. L. Dehmer, J. Chem. Phys. **56**, 4496 (1972), and references therein.

[4]F. A. Gianturco, C. Guidotti, and U. Lamanna, J. Chem. Phys. **57**, 840 (1972).

[5]S. T. Manson and J. W. Cooper, Phys. Rev. **165**, 126 (1968).

[6]J. P. Connerade, Contemp. Phys. **19**, 415 (1978).

[7]K. T. Cheng and C. Froese-Fischer, Phys. Rev. A **28**, 2811 (1983).

[8]K. T. Cheng and W. R. Johnson, Phys. Rev. A **28**, 2820 (1983).

[9]V. P. Sachenko, E. V. Polozhentsev, A. P. Kovtun, Yu. F. Migal, R. V. Vedrinski, and V. V. Kolesnikov, Phys. Lett. **48A**, 169 (1974).

[10]D. Dill and J. L. Dehmer, J. Chem. Phys. **61**, 692 (1974).

[11]J. L. Dehmer and D. Dill, Phys. Rev. Lett. **35**, 213 (1975).

[12]J. L. Dehmer and D. Dill, J. Chem. Phys. **65**, 5327 (1977).

[13]R. S. Wallace, Ph.D. thesis, Boston University, 1980.

[14]D. Loomba, S. Wallace, D. Dill and J. L. Dehmer, J. Chem. Phys. **75**, 4546 (1981).

[15]J. L. Dehmer, D. Dill, and A. C. Parr in *Photophysics and Photochemistry in the Vacuum Ultraviolet,* edited by S. P. McGlynn, G. Findley, and R. Huebner (Reidel, Dordrecht, Holland, 1985), p. 341.

[16]J. Berkowitz, *Photoabsorption, Photoionization, and Photoelectron Spectroscopy* (Academic, New York, 1979).

[17]A. P. Hitchcock and C. E. Brion, Chem. Phys. **37**, 319 (1979).

[18]R. C. C. Perera, J. Barth, R. E. LaVilla, R. D. Deslattes, and A. Henins, Phys. Rev. A **32**, 1489 (1985).

[19]T. Gustafsson, Phys. Rev. A **18**, 1481 (1978).

[20]J. L. Dehmer, A. C. Parr, S. Wallace, and D. Dill, Phys. Rev. A **26**, 3283 (1982).

[21]J.-H. Fock and E. E. Koch, Chem. Phys. **96**, 125 (1985).

[22]L. Ungier and T. D. Thomas, Chem. Phys. Lett. **96**, 247 (1983).

[23]H. W. Haak, G. A. Sawatzky, L. Ungier, J. K. Gimzewski, and T. D. Thomas, Rev. Sci. Instrum. **55**, 696 (1984).

[24]L. Ungier and T. D. Thomas, J. Chem. Phys. **82**, 3146 (1985).

[25]U. Becker, R. Hölzel, H. G. Kerkhoff, B. Langer, D. Szostak, and R. Wehlitz, Phys. Rev. Lett. **56**, 1455 (1986).

[26]C. M. Truesdale, S. H. Southworth, P. H. Kobrin, U. Becker, D. W. Lindle, H. G. Kerkhoff, and D. A. Shirley, Phys. Rev. Lett. **50**, 1265 (1983).

[27]D. Dill, J. R. Swanson, S. Wallace, and J. L. Dehmer, Phys. Rev. Lett. **45**, 1393 (1980).

[28]P. A. Lee and J. B. Pendry, Phys. Rev. B **11**, 2795 (1975).

[29]J. E. Muller and W. L. Schaich, Phys. Rev. B **27**, 6489 (1983).

[30]W. L. Schaich, Phys. Rev. B **29**, 6513 (1984).

[31]J. J. Barton, Ph.D. thesis, University of California, Berkeley, 1985.

[32]C. A. Ashley and S. Doniach, Phys. Rev. B **11**, 1279 (1975).

[33]B. K. Teo, J. Am. Chem. Soc. **103**, 3990 (1981).

[34]J. J. Boland, S. E. Crane, and J. D. Baldeschwieler, J. Chem. Phys. **77**, 142 (1982).

[35]G. Bunker and E. A. Stern, Phys. Rev. Lett. **52**, 1990 (1984).

[36]M. G. White, R. A. Rosenberg, G. Gabor, E. D. Poliakoff, G. Thornton, S. Southworth, and D. A. Shirley, Rev. Sci. Instrum. **50**, 1288 (1979).

[37]S. Southworth, C. M. Truesdale, P. H. Kobrin, D. W. Lindle, W. D. Brewer, and D. A. Shirley, J. Chem. Phys. **76**, 143 (1982).

[38]S. Southworth, U. Becker, C. M. Truesdale, P. H. Kobrin, D. W. Lindle, S. Owaki, and D. A. Shirley, Phys. Rev. A **28**, 261 (1983).

[39]C. N. Yang, Phys. Rev. **74**, 764 (1948).

[40]We note that direct decay to double-ionization (shake-off) channels also is possible, resulting in SF_6^{2+} configurations such as $2p^{-2}$, $2s^{-2}$, $2s^{-1}2p^{-1}$, $2s^{-1}\text{val}^{-1}$, $2p^{-1}\text{val}^{-1}$, and val^{-2}. The energy distribution of the emitted electrons would be very broad and somewhat peaked near 0 eV and the threshold energy for the shake-off process, with the high-energy part of the distribution unresolved from the other components in peak *A* in our TOF spectra. Thus, we cannot assess what percentage of excited neutrals decay directly to shake-off channels at the S $1s \rightarrow 6t_{1u}$ resonance, although we speculate that this fraction probably is less than 20%.

[41]It is important to recall that the peaks enhanced at the S $1s \rightarrow 6t_{1u}$ resonance are not *KLL* Auger peaks, but rather autoionization to photoemission channels. The autoionizing decay of the neutral $SF_6(1s^{-1}6t_{1u})$ state can, however, be described in terms (using Auger notation) similar to those used to describe the Auger decay of the single-ion $SF_6^+(1s^{-1})$.

[42]Some representative examples for relative intensities of atomic and molecular satellites are given in U. Gelius, J. Electron Spectrosc. **5**, 985 (1974).

[43]For the Auger decay of the resonantly produced state, we assume that the $6t_{1u}$ electron is not involved in the decay because other t_{1u} orbitals have more overlap with the S $2p(2t_{1u})$ hole. If the $6t_{1u}$ electron is involved, the S(*LVV*) Auger kinetic energy will shift to even higher energy.

[44]D. A. Shirley, Phys. Rev. A **9**, 1549 (1974).

[45]H. Korber and W. Melhorn, Z. Phys. **191**, 217 (1966); M. O. Krause, T. A. Carlson, and W. E. Moddeman, J. Phys. (Paris) Colloq. **32**, C4-139 (1971).

[46]L. Asplund, P. Kelfve, B. Blomster, H. Siegbahn, and K. Siegbahn, Phys. Scr. **16**, 268 (1977).

[47]In the following analysis, we neglect the previously mentioned direct shake-off decay on resonance, (Ref. 40) which would leave *L*-hole ions which subsequently Auger decay with intensity appearing in the observable S(*LVV*) and S(*LLV*) Auger peaks. As long as the relative abundance of two-core-hole configurations within the shake-off manifold ($2p^{-2}$:$2s^{-2}$:$2p^{-1}2s^{-1}$) is similar to that for the single-ion manifold reached by autoionization ($2p^{-2}v^*$:$2s^{-2}v^*$:$2p^{-1}2s^{-1}v^*$), the qualitative conclusions about the SF_6^+ decay channels are unaffected. Furthermore, double-Auger processes such as $SF_6^+(2p^{-1}) \rightarrow SF_6^{3+}(\text{val}^{-3}) + 2e^-$ are not included in the observed S(*LVV*) and S(*LLV*) Auger peaks. We estimate that off resonance these Auger shake-off processes account for only $\sim 10\%$ of the total *L*-hole Auger decay, based on the measured double Auger processes for *L* holes in Ar (see Ref. 66). On resonance, double Auger decay may occur somewhat more frequently (though single Auger decay probably will still dominate) because highly excited ions like $2p^{-2}6t_{1u}$ undergoing Auger decay may have a greater probability for shaking off the $6t_{1u}$ electron relative to shake-off of a valence electron in the Auger decay of a $2p^{-1}$ ion.

[48]G. Herzberg, *Electronic Spectra and Electronic Structure of Polyatomic Molecules* (Van Nostrand, Princeton, New Jersey, 1966).

[49]K. Siegbahn, C. Nordling, G. Johansson, J. Hedman, P. F. Hedén, K. Hamrin, U. Gelius, T. Bergmark, L. O. Werme, R. Manne, and Y. Baer, *ESCA Applied to Free Molecules* (North-Holland, Amsterdam, London, 1969).

[50]W. Mehlhorn, Z. Phys. **208**, 1 (1968).

[51]J. Vayrynen, R. N. Sodhi, and R. G. Cavell, J. Chem. Phys. **79**, 5329 (1983); M. O. Krause, Phys. Rev. Lett. **34**, 633 (1975).

[52]L. Asplund, P. Kelfve, B. Blomster, H. Siegbahn, K. Siegbahn, R. L. Lozes, and U. I. Wahlgren, Phys. Scr. **16**, 273 (1977); K. Faegri, Jr. and O. Keski-Rahkonen, J. Electron Spectrosc. **11**, 275 (1977).

[53]W. Kronast, R. Huster, and W. Mehlhorn, J. Phys. B **17**, L51 (1984).

[54]Z. M. Goodman, C. D. Caldwell, and M. G. White, Phys. Rev. Lett. **54**, 1156 (1985); **54**, 2381 (1985).

[55]The latest valence ordering, though supported by many-body calculations (Ref. 67), is not completely certain due to the presence of a possible shape resonance affecting *several* valence cross sections at about 23 eV photon energy (Refs. 19–21).

[56]J. A. Stephens and P. Dittman (private communication of calculations by R. S. Wallace).

[57]B. K. Teo and P. A. Lee, J. Am. Chem. Soc. **101**, 2815 (1979).

[58]B. K. Teo, P. A. Lee, A. L. Simons, P. Eisenberger, and B. M. Kincaid, J. Am. Chem. Soc. **99**, 3854 (1977); P. A. Lee, B. K. Teo, and A. L. Simons, *ibid.* **99**, 3856 (1977).

[59]B. X. Yang, J. Kirz, and T. K. Sham, Phys. Lett. **110A**, 301 (1985).

[60]P. A. Lee and G. Beni, Phys. Rev. B **15**, 2862 (1977).

[61]T. A. Ferrett, D. W. Lindle, P. A. Heimann, M. N. Piancastelli, P. H. Kobrin, H. G. Kerkhoff, U. E. Becker, W. D. Brewer, and D. A. Shirley (unpublished).

[62]G. Baym, *Lectures on Quantum Mechanics* (Cummings, Reading, Mass., 1969); A. Messiah, *Quantum Mechanics* (North-Holland, Amsterdam, and Wiley, New York, 1961), Vol. 1.

[63]G. G. B. de Souza, P. Morin, and I. Nenner, J. Chem. Phys. **83**, 492 (1985).

[64]P. Morin, G. G. B. de Souza, I. Nenner, and P. Lablanquie, Phys. Rev. Lett. **56**, 131 (1986).

[65]S. Aksela, K. H. Tan, H. Aksela, and G. M. Bancroft, Phys. Rev. A **33**, 258 (1986).

[66]T. A. Carlson and M. O. Krause, Bull. Am. Phys. Soc. **10**, 455 (1965); Phys. Rev. Lett. **17**, 1079 (1966).

[67]W. von Niessen, L. S. Cederbaum, G. H. F. Diercksen, and G. Hohlneicher, Chem. Phys. **11**, 399 (1975); P. J. Hay, J. Am. Chem. Soc. **99**, 1013 (1977); W. von Niessen, W. P. Kraemer, and G. H. F. Diercksen, Chem. Phys. Lett. **63**, 65 (1979).